Letter

Theory of Mode-Selective Chemistry through Polaritonic Vibrational Strong Coupling

Xinyang Li,* Arkajit Mandal,* and Pengfei Huo*

Cite This: *J. Phys. Chem. Lett.* 2021, 12, 6974–6982

Read Online

ACCESS | Metrics & More | Article Recommendations | Supporting Information

ABSTRACT: Recent experiments have demonstrated remarkable mode-selective reactivities by coupling molecular vibrations with a quantized radiation field inside an optical cavity. The fundamental mechanism behind such effects, on the other hand, remains elusive. In this work, we provide a theoretical explanation of the basic principle of how cavity frequency can be tuned to achieve mode-selective reactivities. We find that the dynamics of the radiation mode leads to a cavity frequency-dependent dynamical caging effect of a reaction coordinate, resulting in suppression of the rate constant. In the presence of competitive reactions, it is possible to preferentially cage a reaction coordinate when the barrier frequencies of competing reactions are different, resulting in a selective slow down of a given reaction. Our theoretical results illustrate the cavity-induced mode-selective chemistry through polaritonic vibrational strong couplings, revealing the fundamental mechanism for changing chemical selectivities through cavity quantum electrodynamics.
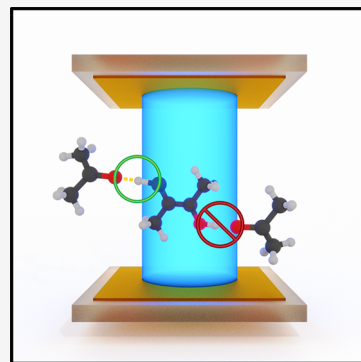
INTRODUCTION

Polariton chemistry is an emerging field[1−5] that provides opportunities for new chemical reactivities and selectivities by coupling molecular systems to quantized radiation fields inside an optical cavity. By hybridizing the vibrational excitations of a molecule with the photonic excitation of the radiation inside the cavity, new light-matter entangled states, so-called polariton states, are generated. Recently, it has been demonstrated that it is possible to suppress[6−10] or enhance[11] ground-state chemical reactivities by placing an ensemble of molecules in an optical microcavity through the resonant coupling between the cavity and vibrational degrees of freedom (DOF) of the molecules, although the validity of the observed enhancement for some experiments[12] is still subject to debate.[12,13] This so-called vibrational strong coupling (VSC) regime[5] operates in the *absence* of any light source[7,8] and was hypothesized to utilize the hybridization of a vibrational transition of a molecule and the zero-point energy fluctuations of a cavity mode.[7,8]

In a recent ground-breaking experiment, Ebbesen and co-workers[7] have demonstrated that the cavity can selectively slow down a particular reaction among competing reaction pathways and revert the reactive selectivities. This new strategy in the VSC regime, if feasible, will allow one to bypass some intrinsic difficulties (such as intramolecular vibrational energy transfer) encountered in the mode-selective chemistry that uses IR excitations to tune chemical reactivities,[14−17] offering a paradigm-shift of synthetic chemistry through cavity-enabled bond-selective chemical transformations.[7,8,18]

Unfortunately, a clear theoretical understanding of such remarkable VSC ground state reactivities remains missing, including an explanation of the resonant effect, in which the suppression of the rate is achieved with a particular cavity photon frequency as well as the collective coupling effects, despite interesting recent progress.[19−23] In addition, the reported branching ratios tilt toward the same product regardless of whether a particular mode is in resonance with the cavity.[7] In particular, with three individual experimental setups that have three different cavity frequencies (associated with particular cavity modes) matching three different bond vibrational frequencies, a similar modification of the branching ratio occurs.[7] This is in contrast to the previous experiments of maximum rate suppression under a specific cavity frequency.[6] A reasonable theoretical explanation for this observed kinetics modification remains elusive.[24]

In response to this theoretical challenge, we have recently conjectured[25] that the radiation mode inside the optical cavity is effectively acting as a "solvent" degree of freedom (DOF) coupled to the molecular reaction coordinate, such that the presence of photonic coordinate enhance the recrossing of the reaction coordinate and reduces the transmission coefficient. This phenomenon is well explored in the context of solvent mediated dynamical caging effects.[26−36] Such effects are *dynamical* and are not captured within a simple transition state theory (TST).[37−40]

In this work, we use the dynamical caging conjecture of VSC polariton chemistry[25] to explore the possibility of cavity-enabled mode-selective chemistry.[7] We consider a model molecular system that has two competing reaction pathways (Reaction 1 and Reaction 2), with a nearly identical potential energy barrier height (with a difference less than 0.4 kcal/mol), but different imaginary barrier frequencies. We demonstrate that by tuning the cavity frequency, one can selectively cage one reaction channel over the other, hence changing the ratio of the rate constants of two reactions as well as the preference of competing reactions. We find that outside the cavity, Reaction 2 is preferred compared to Reaction 1, and by coupling the molecule to the cavity mode within a particular range of frequencies, Reaction 1 is preferred over Reaction 2. Our work thus provides an interesting and tentative explanation for the reversion of the reactive preference by changing the cavity frequency, where a similar behavior has been also observed in recent experiments.[7] However, we must emphasize that our theoretical study is limited to a single molecule coupled to the cavity, whereas the experiment[7] is operated under the collective coupling condition that many molecules are coupled to the cavity. A future theoretical approach is necessary to provide an ultimate answer to the observed VSC modification of reactivities.

CAVITY QUANTUM ELECTRODYNAMICS (QED) HAMILTONIANS

We begin by deriving the quantum light–matter interaction Hamiltonian. The matter Hamiltonian and the corresponding total dipole operator are defined as follows

$$\hat{H}_M = \hat{T} + \hat{V}(\hat{x}) = \sum_j \frac{1}{2m_j}\hat{p}_j^2 + \hat{V}(\hat{x}); \quad \hat{\mu} = \sum_j z_j \hat{x}_j \tag{1}$$

where j is the index of the jth charged particle (including all electrons and nuclei), with corresponding mass m_j and charge z_j. In addition, $\hat{x} \equiv \{\hat{x}_j\} = \{\hat{R}, \hat{r}\}$ with $\hat{R}$ and $\hat{r}$ representing the nuclear and electronic coordinates, respectively, $\hat{p} \equiv \{\hat{p}_R, \hat{p}_r\} \equiv \{\hat{p}_j\}$ is the *mechanical* momentum operator as well as the canonical momentum operator, such that $\hat{p}_j = -i\hbar\nabla_j$. Further, $\hat{T} = \hat{T}_R + \hat{T}_r$ is the kinetic energy operator, where $\hat{T}_R$ and $\hat{T}_r$ represent the kinetic energy operators for nuclei and electrons, respectively, and $\hat{V}(\hat{x})$ is the potential operator that describes the Coulombic interactions among electrons and nuclei.

The cavity photon field Hamiltonian under the single mode assumption is expressed as

$$\hat{H}_{ph} = \hbar\omega_c\left(\hat{a}^\dagger\hat{a} + \frac{1}{2}\right) = \frac{1}{2}(\hat{p}_c^2 + \omega_c^2\hat{q}_c^2) \tag{2}$$

where ω_c is the frequency of the mode in the cavity, $\hat{a}^\dagger$ and $\hat{a}$ are the photonic creation and annihilation operators, and

$$\hat{q}_c = \sqrt{\hbar/2\omega_c}\,(\hat{a}^\dagger + \hat{a})$$

and

$$\hat{p}_c = i\sqrt{\hbar\omega_c/2}\,(\hat{a}^\dagger - \hat{a})$$

are the photonic coordinate and momentum operators, respectively. When the Coulomb gauge, $\nabla\cdot\hat{A} = 0$, is chosen, the vector potential becomes purely transverse $\hat{A} = \hat{A}_\perp$. Under the long-wavelength approximation,

$$\hat{A} = A_0(\hat{a} + \hat{a}^\dagger) = A_0\sqrt{2\omega_c/\hbar}\,\hat{q}_c \tag{3}$$

where

$$A_0 = \sqrt{\frac{\hbar}{2\omega_c\varepsilon_0\mathcal{V}}}\,\hat{e} \equiv A_0\hat{e}$$

for a Fabry–Pérot (FP) cavity, with $\mathcal{V}$ as the quantization volume inside the cavity, ε_0 as the permittivity, and $\hat{e}$ as the unit vector of the field polarization.

The light–matter interaction is described using the minimal coupling QED Hamiltonian (the "p·A" form), which is expressed as

$$\hat{H}_C = \sum_j \frac{1}{2m_j}(\hat{p}_j - z_j\hat{A})^2 + \hat{V}(\hat{x}) + \hat{H}_{ph} \tag{4}$$

We further introduce the Power–Zienau–Woolley (PZW) gauge transformation operator[41,42] as

$$\hat{U} = \exp\left[-\frac{i}{\hbar}\hat{\mu}\cdot\hat{A}\right] = \exp\left[-\frac{i}{\hbar}\hat{\mu}\cdot A_0(\hat{a} + \hat{a}^\dagger)\right] \tag{5}$$

The QED Hamiltonian under the *dipole* gauge (the "d·E" form[41,43]) $\hat{H}_D = \hat{U}\,\hat{H}_C\,\hat{U}^\dagger$ can be obtained by performing the PZW transformation on $\hat{H}_C$ as follows

$$\hat{H}_D = \hat{H}_M + \hbar\omega_c\left(\hat{a}^\dagger\hat{a} + \frac{1}{2}\right) + i\omega_c\hat{\mu}\cdot A_0(\hat{a}^\dagger - \hat{a}) + \frac{\omega_c}{\hbar}(\hat{\mu}\cdot A_0)^2 \tag{6}$$

The last term in eq 6 is commonly referred to as the dipole self-energy (DSE).

The widely used Pauli–Fierz (PF) QED Hamiltonian[44−46] in the dipole gauge in recent studies of polariton chemistry can be obtained using the following unitary transformation

$$\hat{U}_\phi = \exp\left[-i\frac{\pi}{2}\hat{a}^\dagger\hat{a}\right] \tag{7}$$

Applying $\hat{U}_\phi$ on $\hat{H}_D$ leads to the following PF Hamiltonian in the dipole gauge, $\hat{H}_{PF} = \hat{U}_\phi\,\hat{H}_D\,\hat{U}_\phi^\dagger$ as follows

$$\hat{H}_{PF} = \hat{H}_M + \hbar\omega_c\left(\hat{a}^\dagger\hat{a} + \frac{1}{2}\right) + \omega_c\hat{\mu}\cdot A_0(\hat{a} + \hat{a}^\dagger) + \frac{\omega_c}{\hbar}(\hat{\mu}\cdot A_0)^2 \tag{8}$$

One can clearly see that the dipole self-energy term $\frac{\omega_c}{\hbar}(\hat{\mu}\cdot A_0)^2$ is a necessary component in $\hat{H}_D$, originating from $\hat{U}\hat{H}_{ph}\hat{U}^\dagger$. Details of the above derivation are provided in the Supporting Information.

In this work, we explicitly assume that the orientation of the dipole operator is aligned with the field polarization direction $\hat{e}$ such that

$$\hat{\mu}\cdot A_0 = \hat{\mu}A_0 = \hat{\mu}\cdot\sqrt{\frac{\hbar}{2\omega_c\varepsilon_0\mathcal{V}}} \tag{9}$$

where $A_0 = \sqrt{\frac{\hbar}{2\omega_c\varepsilon_0\mathcal{V}}}$ and $\hat{\mu} = \hat{\mu}\cdot\hat{e}$. Future work is needed to explicitly consider the rotational disorder, which treats the above term as $\hat{\mu}\cdot A_0 = \mu\hat{A}_0\cdot\cos\theta$, where θ is the angle between $\hat{\mu}$ and A_0. We expect further inclusion of this effect will reduce the light-matter coupling, but will not qualitatively change the conclusions in this work.

Using $\hat{q}_c$ and $\hat{p}_c$, one can express eq 8 as follows

$$\hat{H}_{PF} = \hat{H}_M + \frac{\hat{p}_c^2}{2} + \frac{1}{2}\omega_c^2\left(\hat{q}_c + \sqrt{\frac{2}{\hbar\omega_c}}A_0\cdot\hat{\mu}(\mathbf{R})\right)^2 \tag{10}$$

Again, the self-energy term $\frac{\omega_c}{\hbar}(\hat{\mu}\cdot A_0)^2$ is a necessary component in $\hat{H}_{PF}$, which originates from $\hat{U}\hat{H}_{ph}\hat{H}^\dagger$ in $\hat{H}_D$ and is preserved from $\hat{H}_D$ to $\hat{H}_{PF}$ under the transformation of $\hat{U}_\phi$ (eq 7). Thus, without DSE, the gauge invariance between the p·A and the d·E forms of the Hamiltonian (including H_D and H_{PF}) will explicitly break down.[45,47−49] This is a well-known result in QED and is revisited in the current literature as well.[47−51]

In this work, we are interested in electronically adiabatic reactions, thus we only consider the electronic ground state defined as

$$(\hat{H}_M - \hat{T}_{\mathbf{R}})|\Psi_g\rangle = E_g(\mathbf{R})|\Psi_g\rangle \tag{11}$$

Projecting $\hat{H}_M$ and $\hat{\mu}$ on the ground electronic state $|\Psi_g\rangle$, we obtain the model Hamiltonian

$$\hat{H} = \frac{\hat{\mathbf{P}}^2}{2M} + E_g(\mathbf{R}) + \frac{\hat{p}_c^2}{2} + \frac{1}{2}\omega_c^2\left(\hat{q}_c + \sqrt{\frac{2}{\hbar\omega_c}}A_0\cdot\mu(\mathbf{R})\right)^2 \tag{12}$$

where $\mu(\mathbf{R}) = \langle\Psi_g|\hat{\mu}|\Psi_g\rangle$ and $E_g(\mathbf{R})$ are defined in eq 11. Note that projecting $\hat{\mu}$ inside the dipole self-energy is the correct matter state truncation scheme for the dipole-gauge Hamiltonian[50,52] as well as for the PF Hamiltonian,[52] because it makes sure all operators are properly confined in the same truncated electronic subspace[52] $\hat{\mathcal{P}} = |\Psi_g\rangle\langle\Psi_g|$ in order to generate consistent and meaningful results. Indeed, if $\hat{\mathcal{I}} = \hat{\mathcal{P}} + \hat{Q}$, then $\hat{\mathcal{P}}\hat{\mu}\hat{\mathcal{P}}$ is properly confined in the subspace $\hat{\mathcal{P}}$, whereas $\hat{\mathcal{P}}\hat{\mu}^2\hat{\mathcal{P}} = \hat{\mathcal{P}}\hat{\mu}(\hat{\mathcal{P}} + \hat{Q})\hat{\mu}\hat{\mathcal{P}}$ contains the terms outside the subspace $\hat{\mathcal{P}}$. More details of this discussion can be found in ref 48 and ref 52.
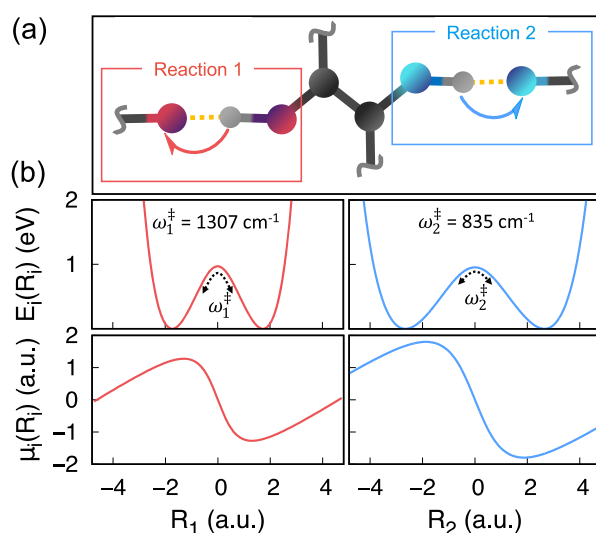
MODEL SYSTEM

In this study, we consider a molecule that can undergo two competing reaction pathways, depicted in Figure 1a. We model these two competing reactions with two independent double-well potentials that are parametrized from the Shin-Metiu-type model together with the corresponding permanent dipoles.[53] This ensures a realistic parameter set for the potential energy surface as well as for the dipole moment. The details on the parameters for the potentials and dipole moments can be found in the Supporting Information. We assume the directions of the two reactions are completely parallel, such that both can be aligned with the cavity polarization direction.

The model molecular Hamiltonian is constructed as

$$E_g(\mathbf{R}) = \sum_{i=1}^{2}\frac{P_i^2}{2M_i} + E(R_1, R_2) + H_{vib} \tag{13}$$

where $M_1 = M_2 = 1836$ au, $E(R_1,R_2) = E_1(R_1) + E_2(R_2)$ is the ground electronic state potential energy surface for two independent double-well potentials, which are depicted in Figure 1b. Further, $\hat{H}_{vib}$ represents the system-bath coupling Hamiltonian that models two separate solvent baths, each coupled to one of the two reaction coordinates. The details of $\hat{H}_{vib}$ are provided in the Supporting Information. In the VSC regime, the cavity mode has a similar range of frequencies as the molecular vibrations, meaning that q_c evolves at a similar time scale as $\mathbf{R}$. Following previous works,[38,39,54] here we treat all nuclear and photonic DOF classically. Further discussions are provided in the Reaction Rate Constant section.

Figure 1. (a) A model molecular system with two competing reactions pathways, labeled as Reaction 1 (red) and Reaction 2 (blue), respectively. (b) The ground state potential energy surfaces (PES) $E_i(R_i)$ are shown in the top panels. The reaction barrier of Reaction 2 ($\omega_2^\ddagger = 835$ cm^{-1}) is much broader than that of Reaction 1 ($\omega_1^\ddagger = 1307$ cm^{-1}). The permanent dipole moments $\mu_i(R_i)$ are shown in the bottom panels. Note that 1 au corresponds to 2.542 D.

The bottom of the well position for the reactant is R_i^0 and the dividing surface position is $R_i^\ddagger$. The reactant well frequency is defined as

$$(\omega_i^0)^2 = \frac{\partial^2 E_i(R_i)}{M_i\partial R_i^2}\Big|_{R_i=R_i^0}$$

and the imaginary barrier frequency is defined as

$$(\omega_i^\ddagger)^2 = -\frac{\partial^2 E_i(R_i)}{M_i\partial R_i^2}\Big|_{R_i=R_i^\ddagger}$$

The total dipole moment is modeled as $\mu(\mathbf{R}) = \mu_1(R_1) + \mu_2(R_2)$. $\mu_i(R_i)$ is the ground state permanent dipole moment of the ith reaction coordinate, depicted in the bottom panels of Figure 1b. We define the slope at the barrier as $\mu_i^{\ddagger'} = \frac{\partial\mu_i(R_i)}{\partial R_i}\Big|_{R_i=R_i^\ddagger}$. In addition, $\hat{H}_{vib}$ (see details in the Supporting Information) is the vibrational system-bath Hamiltonian that describes the interactions between reaction coordinates $\mathbf{R}$ and other phonon modes x in the molecule.

The VSC polariton chemical kinetics can be viewed as a barrier crossing process on the cavity Born−Oppenheimer surface (CBO),[38,44,55]

$$V_{CBO}(\mathbf{R}, q_c) = \sum_{i=1}^{2}E_i(R_i) + \frac{1}{2}\omega_c^2\left(q_c + \sqrt{\frac{2}{\hbar\omega_c}}A_0\cdot\sum_{i=1}^{2}\mu_i(R_i)\right)^2 \tag{14}$$

We further define a normalized coupling strength

$$\tilde{\eta} = \frac{A_0}{\sqrt{M}\hbar} \tag{15}$$

which is used to characterize the coupling strength, and M = 1836 au for the model system used in this work. Note that $\tilde{\eta}$ is a ω_c independent quantity, because inside A_0 (see eq 9) $\mathcal{V} \sim \mathcal{S} \times \omega_c^{-1}$, where $\mathcal{S}$ is the quantization area inside the cavity. Hence, both A_0 as well as $\tilde{\eta}$ are cavity frequency independent.

Throughout this work, we use the value of $\tilde{\eta}$ = 0.047 au. Note that the molecule-cavity coupling strength per molecule used in this work is much stronger than the realistic coupling strength in the VSC experiments[7] that include many molecules. This is because, in these VSC experiments, the collective coupling strength is scaled up by $\sqrt{N}$, which manifests into the observed Rabi splitting in the transmission spectra.[7] With the epsilon-near-zero cavity,[56] it is possible to confine IR frequencies and even achieve an ultrastrong coupling regime. Thus, besides the purely theoretical value of exploring VSC effects on reaction branching ratios, our theoretical simulation is also within reach of near-future experimental setups. Further, we should expect that the difference between the current theoretical work and the VSC experimental work is beyond a simple rescaling of the coupling strength by $\sqrt{N}$. This is because there are other effects from the collective behavior that cannot simply be thought of as scaled-up effects, such as the role of the dark states,[21,23] which could lead to qualitatively different behavior. These are subject to future investigations.

■ REACTION RATE CONSTANT

The rate constant can be rigorously expressed in terms of the TST rate k^{TST} and the transmission coefficient κ as follows

$$k = \lim_{t \to t_p} \kappa(t) \cdot k^{\text{TST}} \tag{16}$$

where t_p refers to the plateau time of the flux-side correlation function, and $\kappa(t)$ is the transmission coefficient that captures dynamical recrossing effects and measures the ratio between the actual reaction rate and the TST rate. We will also refer to the plateau value of the flux-side correlation function as $\kappa(t_p)$. Note that we explicitly consider both the cavity mode q_c as well as the molecular vibrations $\mathbf{R}$ as classical variables, due to their relatively low frequencies. One can explicitly quantize all of these modes through Feynman's imaginary-time path-integral formalism (ring polymer molecular dynamics). We have theoretically explored the effects of quantizing q_c as well as treating it classically in a polariton-mediated electron transfer model system.[57] We found that for cavity frequency ω_c < 200 meV, the classical treatment always yields reasonable results for the ET driving force in the normal regime. Our preliminary tests of RPMD rate constant calculations also confirm that the classical treatment yields similar rate constants as the fully quantized RPMD rate constant. This is beyond the scope of the current work and will be discussed in future works.

In eq 16, the TST rate[35] is expressed as

$$k^{\text{TST}} = \frac{\omega^0}{2\pi} e^{-\beta E^{\ddagger}} \tag{17}$$

where $E^{\ddagger} = E(R^{\ddagger}) - E(R^0)$ is the potential energy barrier height measured from the bottom of the well R^0 to the top of the barrier $R^{\ddagger}$, ω^0 is the vibrational frequency of the reactant at $R = R^0$, and $\beta = (k_B T)^{-1}$. When the DSE is explicitly considered, $E^{\ddagger}$ remains invariant to changes of the light-matter coupling strength or the photon frequency. This is because the equilibrium position along the photonic coordinate q_c is

$$q_c^0(\mathbf{R}) = -\sqrt{\frac{2}{\hbar \omega_c}} A_0 \cdot (\mu_1(R_1) + \mu_2(R_2)) \tag{}$$

for all possible $\mathbf{R}$ (see detailed discussions in the Supporting Information). Thus, the last term in eq 14 is always 0 for the minima or transition state on the CBO surface. This explains

why one cannot observe any effects from a simple TST analysis when treating q_c classically.[39,40,54] A recent work[58] on VSC chemistry that treats q_c quantum mechanically suggests that even when the zero-point energy along q_c is fully considered, the change of $E^{\ddagger}$ is less than 20 cm^{-1} across a large range of coupling strengths.

Since k^{TST} does not change under the VSC condition, we have conjectured[25] that VSC chemical reactivities purely originate from the transmission coefficient κ. In particular, we showed that the reactive coordinate is trapped near the barrier region when it is coupled to a cavity mode.[25] Due to this, the reactive coordinate recrosses the dividing surface multiple times, leading to a reduction in the reactive flux. This effect is also well explored in the context of solvent mediated dynamical caging.[26−36]

We can compute κ through calculating the flux-side correlation function numerically,[59−61] which is defined as

$$\kappa(t) = \frac{\langle \mathcal{F}(0) \cdot h[R(t) - R^{\ddagger}] \rangle}{\langle \mathcal{F}(0) \cdot h[\dot{R}^{\ddagger}(0)] \rangle} \tag{18}$$

where $h[R - R^{\ddagger}]$ is a Heaviside function of the reaction coordinate R and the dividing surface $R^{\ddagger}$ that separates the reactant and the product, $\mathcal{F}(t) = \dot{h}(t) = \delta[R(t) - R^{\ddagger}] \cdot \dot{R}(t)$ is the flux function that measures the reactive flux across the dividing surface (with $\delta(R)$ as the Dirac delta function), and $\langle \cdots \rangle$ represents the canonical ensemble average (subject to the constraint on the dividing surface which is enforced by $\delta[R(t) - R^{\ddagger}]$ inside $\mathcal{F}(t)$). Further, $\dot{R}^{\ddagger}(0)$ represents the initial velocities of the nuclei on the dividing surface. A total of 100 000 configurations are sampled with the constraint on the dividing surface, which are then released with the initial velocities randomly sampled from the classical Maxwell−Boltzmann distribution. Each trajectory is propagated for 450 fs, which guarantees that the flux-side correlation function will plateau. The numerical simulation details of κ are provided in the Supporting Information.

We should also emphasize that we consider a perfect cavity setup with no photon loss (photon leaking of the cavity). Despite the recent progress in the development of high quality-factor Fabry-Pérot cavities, optical microcavities are generally lossy. The typical values of cavity losses for a Fabry-Pérot cavity is in the range of 5−100 meV.[7,62−64] However, we expect the cavity loss will further assist the dynamical caging effect, because the cavity loss can be modeled with an additional dissipative noncavity bath coupled to the cavity mode.[65] With such an additional bath coupled to the cavity mode, one should expect an increase of the dissipation from the reactive molecule, leading to the further reduction of reactive flux. This effect will be explored in the future.

Further, the total rate constant of the model system can be calculated from the Grote−Hynes (GH) Rate Theory.[29,66,67] The GH rate constant is given as[35,67−69]

$$k^{\text{GH}} = \frac{1}{2\pi} \frac{\prod_{\nu=1}^{N} \Omega_{\nu}^0}{\prod_{\nu=2}^{N} \Omega_{\nu}^{\ddagger}} e^{-\beta E^{\ddagger}} \tag{19}$$

where $\{\Omega_{\nu}^0\}$ are the normal-mode frequencies of the Hamiltonian in the reactant well, and for $\nu \geq 2$, $\{\Omega_{\nu}^{\ddagger}\}$ are the stable normal-mode frequencies of the transition state, such that $\Omega_{\nu}^{\ddagger 2} > 0$. For $\nu = 1$, $\Omega_{\nu}^{\ddagger 2} < 0$ is the imaginary frequency of the transition state. Treating $\mathbf{R}$ and q_c as the "coordinates" of the hybrid system, we directly diagonalize the Hessian matrix of the model Hamiltonian (eq 14) to compute these frequencies to

obtain the GH rate. The details of these calculations are provided in the Supporting Information.

The yield of the reaction i is estimated as[7]

$$\phi_i = \frac{k_i}{k_1 + k_2} \tag{20}$$

for two competing pathways $i \in \{1,2\}$, where the reaction rate constants $k_i = \kappa_i(t_p) \cdot k_i^{\mathrm{TST}}$, $\kappa(t_p)$ can be computed based on eq 17 and eq 18, or using the GH analytical rate theory in eq 19.

■ RESULTS AND DISCUSSION

Figure 2a presents the reaction rate constants k_i of two competing pathways $i \in \{1,2\}$ as a function of cavity frequency
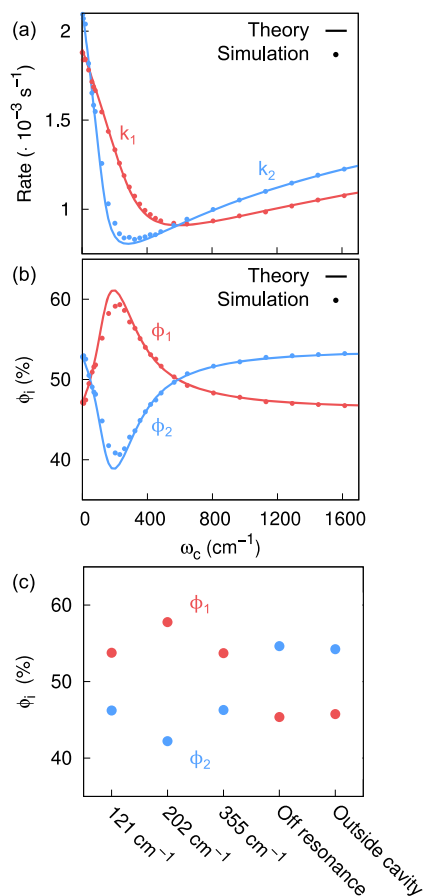
Figure 2. (a) The chemical reaction rate constants of the two competing pathways 1 (red) and 2 (blue) at various cavity frequencies ω_c obtained from numerical simulations (dots) based on eq 16 as well as the analytical rate expression (solid lines) in eq 19. (b) The yield (%) ϕ_i (eq 20) of reaction i as a function of ω_c. The preference of the product is reversed in the region of $\omega_c \in [49 \text{ cm}^{-1}, 565 \text{ cm}^{-1}]$. (c) Several representative ϕ_i at various cavity frequencies and outside the cavity.

ω_c under the normalized coupling strength (see eq 15) $\tilde{\eta} = 0.047$ au. One can clearly see that the two reaction rate constants k_1 and k_2 are suppressed in the presence of the cavity, agreeing with the recently observed rate constant suppression in VSC chemistry. We emphasize that the suppression completely originates from the reduction of the transmission coefficient κ (eq 18), not from the TST rate constant (eq 17), as the classical barrier height does not change in the presence of a cavity. Interestingly, the maximum suppression of k_i occurs at two

different cavity frequencies. This cavity frequency-dependent reduction of the rate constant has been explained from our earlier work:[25] when the cavity frequency reaches a frequency related to the top of the barrier frequency $\omega_i^{\ddagger}$, the dynamical caging effect reaches its largest magnitude. More specifically, for a simplified model with only one reaction coordinate and without the phonon bath $\hat{H}_{\mathrm{vib}}$ (in eq 13), the maximum suppression frequency is

$$\omega_i^s = -\frac{\hbar}{2}\tilde{\eta}^2(\mu_i^{\ddagger\prime})^2 + \frac{1}{2}\sqrt{\hbar^2\tilde{\eta}^4(\mu_i^{\ddagger\prime})^4 + 4\omega_i^{\ddagger 2}} \tag{21}$$

where

$$\mu_i^{\ddagger\prime} = \frac{\partial \mu_i(R_i))}{\partial R_i}\Big|_{R_i = R_i^{\ddagger}}$$

The presence of $\hat{H}_{\mathrm{vib}}$ does not significantly change this frequency. The detailed derivation and discussions are provided in the Supporting Information. When $\tilde{\eta}$ is small such that $\tilde{\eta}^4(\mu_i^{\ddagger\prime})^4 \ll 4\omega_i^{\ddagger 2}$, the maximum suppression frequency is close to the barrier frequency ($\omega^s \approx \omega_i^{\ddagger}$). When the coupling strength $\tilde{\eta}$ increases, the minimum is shifted to the low-frequency region, as demonstrated by the scenario in Figure 2a. Note that this is the general trend of ω_i^s based on eq 21. Throughout the paper, we keep the coupling strength fixed at $\tilde{\eta} = 0.047$ au. Nevertheless, the difference in $\omega_i^{\ddagger}$ of the two competing reactions manifests into the difference in the maximum suppression frequencies associated with the two reactions.

Note that under the limit where the cavity frequency is highly off-resonance with respect to the relevant molecular frequencies, the rate constant will be the same compared to the case where a molecule is outside of a cavity, including when the cavity frequency is very low or very high relative to the molecular vibrational frequencies. This is indeed the case, and the additional results of the rate constant with $\omega_c > 1600 \text{ cm}^{-1}$ are provided in the Supporting Information. However, with the classical treatment of the photonic DOF, it requires a high photon frequency ($>8000 \text{ cm}^{-1}$) for the rate constant to match the value of the outside cavity case. We expect that when treating the cavity DOF quantum mechanically, the transmission coefficient will recover the cavity-free value at a much lower cavity frequency, resulting in a much sharper dip in the frequency dependent transmission coefficient profile (similar to the experimental results[6]).

We must emphasize that the VSC experiments[6,7,9] suggest that under the condition $\omega_i^{\ddagger} \approx \omega_i^0$ (bottom of the well frequency), the rate achieves maximum suppression. Thus, unless for systems that have $\omega_i^0 \approx \omega_{\ddagger}^0$ (such as the model potential used in this study), the current theory gives a different prediction of the resonant suppression compared to the experiments.

Figure 2b presents the yield of the product ϕ_i (defined in eq 20) for reaction i as a function of ω_c. As one can see, the changing preference of the product is rooted in the frequency-dependent suppression of the rate constant k_i shown in Figure 2b. In particular, the reverted preference occurs at a range of different cavity frequencies, in the region of $\omega_c \in [49 \text{ cm}^{-1}, 565 \text{ cm}^{-1}]$, and the maximum reverted preference occurs at $\omega_c = 201.6 \text{ cm}^{-1}$, at which the ratio k_2/k_1 has been changed the most significantly by coupling to the cavity (because $\phi_1 = 1/(1 + k_2/k_1)$). Even though our model system is different than the molecular system explored by Ebbesen and co-workers,[7] and the molecule-cavity coupling scenario is different (single molecule

in the current study versus many-molecules collective coupling in the experiments), our results do show some interesting basic features similar to those discovered in the experiments.[7]

Figure 2c presents several representative data points. In particular, we find that using a high-frequency off-resonant cavity (ω_c is larger than all vibrational frequencies, such as $\omega_c >$ 1600 cm^{-1} in the current model), the selectivity is the same as the original selectivity without the cavity (effectively $\omega_c = 0$). Further, we find that the reverted preference occurs during *a range of cavity frequencies*, even though the maximum reduction of the rate constants for two competing reactions occurs at *two specific cavity frequencies*. Our theoretical results provide a new perspective to understand the recent VSC enhanced selectivities of competing reactions, such as the results presented in ref 7 (in particular, Figure 3b in that work). To further understand the reverted selectivities of reactions, we explore representative reactive trajectories on the CBO surfaces for both reactions.
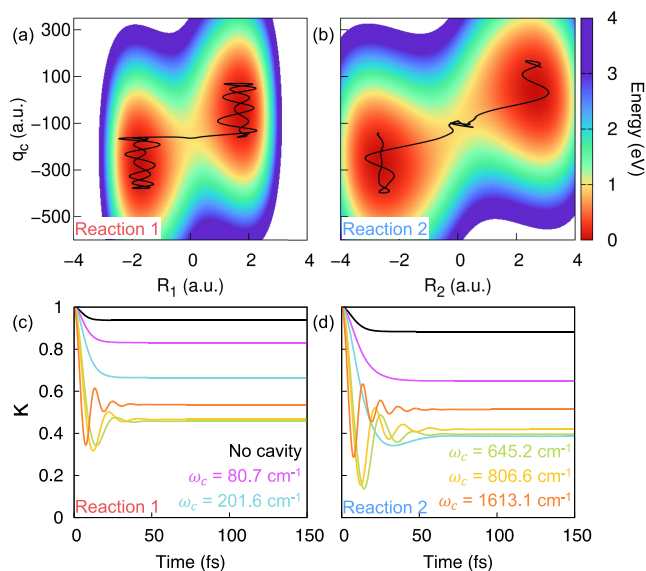
Figure 3. (a) The Cavity Born−Oppenheimer (CBO) surface (defined in eq 14) and a representative reactive trajectory for Reaction 1 at $\omega_c = $ 201.6 cm^{-1}. The reaction coordinate R_2 is fixed at its equilibrium position for plotting the CBO surface, while in the numerical simulations, it is fluctuating in its reactant well during the course of Reaction 1. (b) CBO surface for Reaction 2 at $\omega_c = 201.6$ cm^{-1}, which exhibits the dynamical caging effect from the photon field (recrossing in the barrier region). The transmission coefficient $\kappa(t)$ at various cavity frequencies ω_c are presented for (c) Reaction 1 and (d) Reaction 2.

Figure 3a presents the CBO surface along the photonic coordinate q_c as well as reactive coordinate R_1, whereas R_2 is fixed at the equilibrium position R_2^0. The molecule is coupled to a cavity with $\omega_c = 201.6$ cm^{-1} through coupling strength $\tilde{\eta} = 0.047$ au. A representative trajectory for the molecule undergoing Reaction 1 (black solid line) is also presented on top of the CBO surface. Because ω_c is detuned from the maximum suppression frequency ω_1^s (eq 21), the friction from the photonic coordinate q_c does not severely impede the transitions of R_1. The majority of the trajectories of Reaction 1 directly pass through the transition state region such that the transmission coefficient κ_1 is not significantly reduced compared to the value in the no-coupling case.

Figure 3b presents the CBO surface along q_c and R_2, as well as a representative reactive trajectory for Reaction 2 under the

same cavity frequency and coupling strength used in Figure 3a. For Reaction 2, the cavity frequency ω_c is close to the maximum suppression frequency ω_2^s, and the reaction coordinate R_2 becomes trapped in a narrow "solvent cage" on the barrier top, hence significantly lowering κ_2 through multiple recrossing dynamics (as shown in Figure 3b). Together with Figure 3a, we find that the *fundamental mechanism* of the cavity-enhanced selectivities originates from a *selective dynamical caging effect* (i.e., enhancement of the recrossing dynamics) among two competing reactions, which occurs when the cavity frequency is selectively tuned to match the maximum suppression frequency ω_i^s of one reaction, but not the other.

Figure 3c,d presents the time-dependent transmission coefficient $\kappa(t)$ (see eq 18) for (c) Reaction 1 and (d) Reaction 2 at five different cavity frequencies. Note that as ω_c increases, $\kappa(t)$ for both reactions becomes more oscillatory. The long-time plateau values of $\kappa(t_p)$ decrease with increasing cavity frequency. After reaching a minimum (when $\omega_c = \omega_i^s$ for a given reaction), $\kappa(t_p)$ starts to increase again. This can be clearly seen from the rate constant presented in Figure 2. This cavity-frequency-dependent suppression of the rate constant has been extensively discussed in our previous work:[25] when ω_c is close to ω_i^s, the dynamical caging effect reaches its maximum magnitude, and when ω_c deviates from ω_i^s, the reactive channel on the CBO surface is either very broad or very narrow, such that the reactive trajectory is not severely caged compared to the condition of $\omega_c = \omega_i^s$.

Figure 4 presents the temperature dependence of the rate constant based on the analytic result k_{GH} (eq 19) for (a)
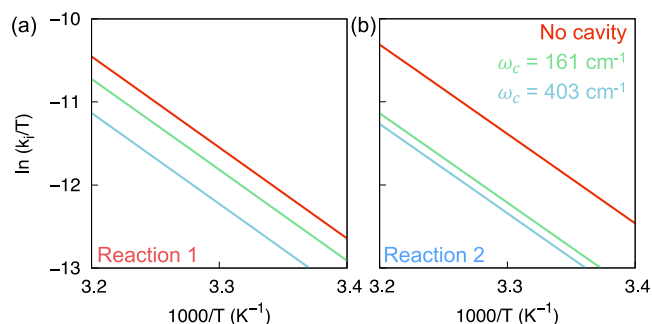
Figure 4. Eyring plot of the reaction rate constant based on the analytic result k_{GH} (eq 19) for (a) Reaction 1 and (b) Reaction 2. The coupling strength is fixed at $\tilde{\eta} = 0.047$ au. The molecule is put outside cavity (red) or within the cavity with a frequency of $\omega_c = 161$ cm^{-1} (green) or $\omega_c = 355$ cm^{-1} (blue). The temperature range is between 294 and 313 K.

Reaction 1 and (b) Reaction 2, over a range of temperatures from 294 to 313 K. Here, we fix the coupling strength $\tilde{\eta} = 0.047$ au and choose three conditions: (i) outside the cavity (red), (ii) inside the cavity with $\omega_c = 161$ cm^{-1} (green), and (iii) inside the cavity with $\omega_c = 355$ cm^{-1} (blue). Recall that the simple Eyring theory gives

$$\ln \frac{k}{T} = -\frac{\Delta H^{\ddagger}}{k_B} \cdot \frac{1}{T} + \frac{\Delta S^{\ddagger}}{k_B} + \ln \frac{k_B}{h} \tag{22}$$

where $h = 2\pi\hbar$ is the Planck constant, and $\Delta H^{\ddagger}$ and $\Delta S^{\ddagger}$ are the activation enthalpy and entropy (per molecule), respectively. Hence, $-\frac{\Delta H^{\ddagger}}{k_B}$ gives the effective slope of the Eyring plot and $\frac{\Delta S^{\ddagger}}{k_B} + \ln \frac{k_B}{h}$ is the intercept on the y axis.

On the basis of our current theoretical hypothesis of the dynamical caging effect, we provide the following explanation of the site-selective chemistry.[7] Outside the cavity, Reaction 2 has a larger rate constant as it has a lower reaction barrier compared to Reaction 1 (by around 0.4 kcal/mol). When coupling to the cavity with the frequency in the "preference reversion region" (see Figure 2), Reaction 2 is more suppressed than Reaction 1 due to the selective dynamical caging effect. If one chooses to use the Eyring equation (eq 22), this rate constant reduction is reflected as the decrease of the entropy change $\Delta S^{\ddagger}$. On the other hand, the barrier height $E^{\ddagger}$ for the light-matter hybrid system does not change with respect to the cavity frequency, hence the slope of the Eyring plot $-\frac{\Delta H^{\ddagger}}{k_B}$ does not change upon coupling to the cavity in our current theoretical studies. Our results reproduce some basic features in the experimental work of Ebbesen and co-workers,[7] providing an interesting explanation of the observed activation entropy reduction when coupling reactive molecules to the cavity (such as Figure 4 in ref 7) from the dynamical caging effect. However, the current theory cannot explain the change of slope in the Eyring plot observed in the experiments,[7] and future theoretical development is required to fully understand the observed modifications of kinetics.

CONCLUSIONS

In this work, we demonstrate the possibility of cavity-enabled mode-selective chemistry originating from the *dynamical caging* effect from the photon field, which causes maximum suppression of a reaction rate constant at a frequency related to the original imaginary barrier frequency of the reaction pathway. We show that the ratio of the two rate constants, hence, the selectivity of two competing reaction pathways can be reverted when the two pathways have different barrier frequencies. This is because under a specific cavity frequency, one reaction is not as caged as the other one due to a difference in their imaginary barrier frequencies. Under strong light-matter coupling strengths, the preferred products can be reverted at a range of cavity frequencies. The reactive preference when the cavity frequency is much higher than all vibrational frequencies (off-resonant condition) remains the same as the original preference outside the cavity. These findings reproduce the basic features observed in the recent experiments.[7]

Admittedly, the cavity frequencies where maximum suppression occurs show a strong redshift with respect to the original barrier frequencies of both pathways, due to the large coupling strength we chose. As we explained in our previous work,[25] the experiments are in the collective coupling regime,[7] whereas our work is limited to the case where a few molecules are strongly coupled to a single radiation mode. The open question for future investigation is whether the present caging effect still survives in the case of collective coupling in the VSC regime, where many molecules couple to a Fabry-Pérot cavity and the light–matter coupling strength per molecule is very weak. Future theoretical work is needed to be done to investigate the collective effects in the VSC regime.[39,54] The basic feature of branching ratio reversion due to selective suppression of the rate constant (Figure 2) might remain a valid explanation for the reaction branching ratios over a range of cavity frequencies under the future theory that can explain the collective coupling and the resonant reduction of the rate constant at the bond vibrational frequency. On the other hand, with an epsilon-near-zero cavity,[56] it is possible to confine IR frequencies and even

achieve an ultrastrong coupling regime. Thus, it might be possible to directly verify our theoretical predictions in the near future for the case of a single molecule or a few molecules strongly coupled to the cavity.

To summarize, our work provides a plausible theoretical explanation for mode-selective chemistry through polaritonic vibrational strong coupling. The rate constants of two competing reactions are unevenly suppressed from the dynamical caging effect originating from the molecule–cavity interactions. Further investigation will focus on understanding the collective VSC reactivities by coupling many molecules with the cavity.[39,54]

■ ASSOCIATED CONTENT

ⓢ Supporting Information

The Supporting Information is available free of charge at https://pubs.acs.org/doi/10.1021/acs.jpclett.1c01847.

> Details of the derivation of the Pauli-Fierz QED Hamiltonian, model molecular Hamiltonian, parameterization of the electronic ground state and dipole, details of the Grote–Hynes theory, cavity-frequency dependence of the rate constant, and computational details (PDF)

■ AUTHOR INFORMATION

Corresponding Authors

  Xinyang Li — *Department of Chemistry, University of Rochester, Rochester, New York 14627, United States;* Email: xinyang.li@rochester.edu

  Arkajit Mandal — *Department of Chemistry, University of Rochester, Rochester, New York 14627, United States;* ⓞ orcid.org/0000-0001-9088-2980; Email: amandal4@ur.rochester.edu

  Pengfei Huo — *Department of Chemistry and Institute of Optics, University of Rochester, Rochester, New York 14627, United States;* ⓞ orcid.org/0000-0002-8639-9299; Email: pengfei.huo@rochester.edu

Complete contact information is available at:
https://pubs.acs.org/10.1021/acs.jpclett.1c01847

Notes
The authors declare no competing financial interest.

■ REFERENCES

(1) Ebbesen, T. W. Hybrid Light-matter States in a Molecular and Material Science Perspective. *Acc. Chem. Res.* **2016**, *49*, 2403−2412.

(2) Ribeiro, R. F.; Martínez-Martínez, L. A.; Du, M.; Campos-Gonzalez-Angulo, J.; Yuen-Zhou, J. Polariton Chemistry: Controlling Molecular Dynamics with Optical Cavities. *Chem. Sci.* **2018**, *9*, 6325−6339.

(3) Feist, J.; Galego, J.; Garcia-Vidal, F. J. Polaritonic Chemistry with Organic Molecules. *ACS Photonics* **2018**, *5*, 205−216.

(4) Herrera, F.; Owrutsky, J. Molecular Polaritons for Controlling Chemistry with Quantum Optics. *J. Chem. Phys.* **2020**, *152*, 100902.

(5) Hirai, K.; Hutchison, J. A.; Uji-i, H. Recent Progress in Vibropolaritonic Chemistry. *ChemPlusChem* **2020**, *85*, 1981−1988.

(6) Thomas, A.; George, J.; Shalabney, A.; Dryzhakov, M.; Varma, S. J.; Moran, J.; Chervy, T.; Zhong, X.; Devaux, E.; Genet, C.; et al. Ground-state Chemical Reactivity under Vibrational Coupling to the Vacuum Electromagnetic Field. *Angew. Chem.* **2016**, *128*, 11634−11638.

(7) Thomas, A.; Lethuillier-Karl, L.; Nagarajan, K.; Vergauwe, R. M. A.; George, J.; Chervy, T.; Shalabney, A.; Devaux, E.; Genet, C.; Moran, J.; et al. Tilting a Ground-state Reactivity Landscape by Vibrational Strong Coupling. *Science* **2019**, *363*, 615−619.

(8) Thomas, A.; Jayachandran, A.; Lethuillier-Karl, L.; Vergauwe, R. M.; Nagarajan, K.; Devaux, E.; Genet, C.; Moran, J.; Ebbesen, T. W. Ground State Chemistry under Vibrational Strong Coupling: Dependence of Thermodynamic Parameters on the Rabi Splitting Energy. *Nanophotonics* **2020**, *9*, 249−255.

(9) Vergauwe, R. M. A.; Thomas, A.; Nagarajan, K.; Shalabney, A.; George, J.; Chervy, T.; Seidel, M.; Devaux, E.; Torbeev, V.; Ebbesen, T. W. Modification of Enzyme Activity by Vibrational Strong Coupling of Water. *Angew. Chem., Int. Ed.* **2019**, *58*, 15324−15328.

(10) Hirai, K.; Takeda, R.; Hutchison, J. A.; Uji-i, H. Modulation of Prins Cyclization by Vibrational Strong Coupling. *Angew. Chem., Int. Ed.* **2020**, *59*, 5332−5335.

(11) Lather, J.; Bhatt, P.; Thomas, A.; Ebbesen, T. W.; George, J. Cavity Catalysis by Cooperative Vibrational Strong Coupling of Reactant and Solvent Molecules. *Angew. Chem., Int. Ed.* **2019**, *58*, 10635−10638.

(12) Hiura, H.; Shalabney, A. Vacuum-field Catalysis: Accelerated Reactions by Vibrational Ultra Strong Coupling. *ChemRxiv* **2019**, in-press.

(13) Imperatore, M. V.; Asbury, J. B.; Giebink, N. C. Reproducibility of Cavity-enhanced Chemical Reaction Rates in the Vibrational Strong Coupling Regime. *J. Chem. Phys.* **2021**, *154*, 191103.

(14) Zewail, A. H. Laser Selective Chemistry−Is It Possible? *Phys. Today* **1980**, *33*, 27−33.

(15) Frei, H.; Pimentel, G. C. Selective Vibrational Excitation of the Ethylene-fluorine Reaction in a Nitrogen Matrix. I. *J. Chem. Phys.* **1983**, *78*, 3698−3712.

(16) Frei, H. Selective Vibrational Excitation of the Ethylene-fluorine Reaction in a Nitrogen Matrix. Ii. *J. Chem. Phys.* **1983**, *79*, 748−758.

(17) Zare, R. N. Laser Control of Chemical Reactions. *Science* **1998**, *279*, 1875−1879.

(18) Kéna-Cohen, S.; Yuen-Zhou, J. Polariton Chemistry: Action in the Dark. *ACS Cent. Sci.* **2019**, *5*, 386−388.

(19) Campos-Gonzalez-Angulo, J. A.; Ribeiro, R. F.; Yuen-Zhou, J. Resonant Catalysis of Thermally Activated Chemical Reactions with Vibrational Polaritons. *Nat. Commun.* **2019**, *10*, 4685.

(20) Schafer, C.; Flick, J.; Ronca, E.; Narang, P.; Rubio, A. Shining Light on the Microscopic Resonant Mechanism Responsible for Cavity-mediated Chemical Reactivity. *arXiv:2104.12429*, https://arxiv.org/abs/2104.12429, 2021.

(21) Li, T. E.; Nitzan, A.; Subotnik, J. E. Collective Vibrational Strong Coupling Effects on Molecular Vibrational Relaxation and Energy Transfer: Numerical Insights via Cavity Molecular Dynamics Simulations. *Angew. Chem., Int. Ed.* **2021**, *60*, 15533−15540.

(22) Li, T. E.; Nitzan, A.; Subotnik, J. E. Energy-efficient Pathway for Selectively Exciting Solute Molecules to High Vibrational States via Solvent Vibration-polariton Pumping. *arXiv:2104.15121*, https://arxiv.org/abs/2104.15121, 2021.

(23) Du, M.; Yuen-Zhou, J. Can Dark States Explain Vibropolaritonic Chemistry? *arXiv:2104.07214*, https://arxiv.org/abs/2104.07214, 2021.

(24) Climent, C.; Feist, J. On the Sn2 Reactions Modified in Vibrational Strong Coupling Experiments: Reaction Mechanisms and Vibrational Mode Assignments. *Phys. Chem. Chem. Phys.* **2020**, *22*, 23545−23552.

(25) Li, X.; Mandal, A.; Huo, P. Cavity frequency-dependent theory for vibrational polariton chemistry. *Nat. Commun.* **2021**, *12*, 1315.

(26) Peters, B. *Reaction Rate Theory and Rare Event*; Elsevier: Amsterdam, NL, 2017.

(27) Bergsma, J. P.; Gertner, B. J.; Wilson, K. R.; Hynes, J. T. Molecular Dynamics of a Model S$_N$2 Reaction in Water. *J. Chem. Phys.* **1987**, *86*, 1356−1376.

(28) Keirstead, W. P.; Wilson, K. R.; Hynes, J. T. Molecular Dynamics of a Model S$_N$1 Reaction in Water. *J. Chem. Phys.* **1991**, *95*, 5256−5267.

(29) Ciccotti, G.; Ferrario, M.; Hynes, J. T.; Kapral, R. Dynamics of Ion Pair Interconversion in a Polar Solvent. *J. Chem. Phys.* **1990**, *93*, 7137−7147.

(30) Tolokh, I. S.; White, G. W. N.; Goldman, S.; Gray, C. G. Prediction of Ion Channel Transport from Grote-Hynes and Kramers Theories. *Mol. Phys.* **2002**, *100*, 2351−2359.

(31) Roca, M.; Moliner, V.; Tuñón, I.; Hynes, J. T. Coupling between Protein and Reaction Dynamics in Enzymatic Processes: Application of Grote-Hynes Theory to Catechol O-Methyltransferase. *J. Am. Chem. Soc.* **2006**, *128*, 6186−6193.

(32) Kanaan, N.; Roca, M.; Tunon, I.; Marti, S.; Moliner, V. Application of Grote-Hynes Theory to the Reaction Catalyzed by Thymidylate Synthase. *J. Phys. Chem. B* **2010**, *114*, 13593−13600.

(33) van der Zwan, G.; Hynes, J. T. Dynamical Polar Solvent Effects on Solution Reactions: A Simple Continuum Model. *J. Chem. Phys.* **1982**, *76*, 2993−3001.

(34) Gertner, B. J.; Wilson, K. R.; Hynes, J. T. Nonequilibrium Solvation Effects on Reaction Rates for Model S$_N$2 Reactions in Water. *J. Chem. Phys.* **1989**, *90*, 3537−3558.

(35) Hänggi, P.; Talkner, P.; Borkovec, M. Reaction-rate Theory: Fifty Years After Kramers. *Rev. Mod. Phys.* **1990**, *62*, 251−341.

(36) Henriksen, N. E.; Hansen, F. Y. *Theories of Molecular Reaction Dynamics: The Microscopic Foundation of Chemical Kinetics*; Oxford Univ. Press: Oxford, UK, 2008.

(37) Li, T. E.; Chen, H.-T.; Nitzan, A.; Subotnik, J. E. Quasiclassical Modeling of Cavity Quantum Electrodynamics. *Phys. Rev. A: At., Mol., Opt. Phys.* **2020**, *101*, 033831.

(38) Galego, J.; Climent, C.; Garcia-Vidal, F. J.; Feist, J. Cavity Casimir-Polder Forces and Their Effects in Ground-state Chemical Reactivity. *Phys. Rev. X* **2019**, *9*, 021057.

(39) Campos-Gonzalez-Angulo, J. A.; Yuen-Zhou, J. Polaritonic Normal Modes in Transition State Theory. *J. Chem. Phys.* **2020**, *152*, 161101.

(40) Zhdanov, V. P. Vacuum Field in a Cavity, Light-mediated Vibrational Coupling, and Chemical Reactivity. *Chem. Phys.* **2020**, *535*, 110767.

(41) Power, E. A.; Zienau, S. Coulomb Gauge in Non-relativistic Quantum Electro-dynamics and the Shape of Spectral Lines. *Philos. Trans. R. Soc. London, Ser. A* **1959**, *251*, 427−454.

(42) Cohen-Tannoudji, C.; Dupont-Roc, J.; Grynberg, G. *Photons and Atoms: Introduction to Quantum Electrodynamics*; John Wiley & Sons, Inc.: Hoboken, NJ, 1989.

(43) Göppert-Mayer, M. Elementary Processes with Two Quantum Transitions. *Ann. Phys. (Berlin, Ger.)* **2009**, *18*, 466−479.

(44) Flick, J.; Ruggenthaler, M.; Appel, H.; Rubio, A. Atoms and Molecules in Cavities, from Weak to Strong Coupling in Quantum-electrodynamics (QED) Chemistry. *Proc. Natl. Acad. Sci. U. S. A.* **2017**, *114*, 3026.

(45) Rokaj, V.; Welakuh, D. M.; Ruggenthaler, M.; Rubio, A. Light−matter Interaction in the Longwavelength Limit: No Ground-state without Dipole Self-energy. *J. Phys. B: At., Mol. Opt. Phys.* **2018**, *51*, 034005.

(46) Schäfer, C.; Ruggenthaler, M.; Rubio, A. Ab Initio Nonrelativistic Quantum Electrodynamics: Bridging Quantum Chemistry and Quantum Optics from Weak to Strong Coupling. *Phys. Rev. A: At., Mol., Opt. Phys.* **2018**, *98*, 043801.

(47) Frisk Kockum, A.; Miranowicz, A.; De Liberato, S.; Savasta, S.; Nori, F. Ultrastrong Coupling between Light and Matter. *Nat. Rev. Phys.* **2019**, *1*, 19−40.

(48) Di Stefano, O.; Settineri, A.; Macri, V.; Garziano, L.; Stassi, R.; Savasta, S.; Nori, F. Resolution of Gauge Ambiguities in Ultrastrong-coupling Cavity Quantum Electrodynamics. *Nat. Phys.* **2019**, *15*, 803−808.

(49) Schäfer, C.; Ruggenthaler, M.; Rokaj, V.; Rubio, A. Relevance of the Quadratic Diamagnetic and Self-polarization Terms in Cavity Quantum Electrodynamics. *ACS Photonics* **2020**, *7*, 975−990.

(50) De Bernardis, D.; Pilar, P.; Jaako, T.; De Liberato, S.; Rabl, P. Breakdown of Gauge Invariance in Ultrastrong-coupling Cavity QED. *Phys. Rev. A: At., Mol., Opt. Phys.* **2018**, *98*, 053819.

(51) Mandal, A.; Krauss, T. D.; Huo, P. Polariton-mediated Electron Transfer via Cavity Quantum Electrodynamics. *J. Phys. Chem. B* **2020**, *124*, 6321−6340.

(52) Taylor, M. A. D.; Mandal, A.; Zhou, W.; Huo, P. Resolution of Gauge Ambiguities in Molecular Cavity Quantum Electrodynamics. *Phys. Rev. Lett.* **2020**, *125*, 123602.

(53) Shin, S.; Metiu, H. Nonadiabatic Effects on the Charge Transfer Rate Constant: A Numerical Study of a Simple Model System. *J. Chem. Phys.* **1995**, *102*, 9285−9295.

(54) Li, T. E.; Nitzan, A.; Subotnik, J. E. On the Origin of Ground-state Vacuum-field Catalysis: Equilibrium Consideration. *J. Chem. Phys.* **2020**, *152*, 234107.

(55) Flick, L. J.; Appel, H.; Ruggenthaler, M.; Rubio, A. Cavity Born-Oppenheimer Approximation for Correlated Electron-Nuclear-Photon Systems. *J. Chem. Theory Comput.* **2017**, *13*, 1616−1625.

(56) Yoo, D.; de León-Pérez, F.; Pelton, M.; Lee, I.-H.; Mohr, D. A.; Raschke, M. B.; Caldwell, J. D.; Martín-Moreno, L.; Oh, S.-H. Ultrastrong Plasmon-phonon Coupling via Epsilon-near-zero Nanocavities. *Nat. Photonics* **2021**, *15*, 125−130.

(57) Chowdhury, S. N.; Mandal, A.; Huo, P. Ring Polymer Quantization of the Photon Field in Polariton Chemistry. *J. Chem. Phys.* **2021**, *154*, 044109.

(58) Fischer, E. W.; Saalfrank, P. Ground State Properties and Infrared Spectra of Anharmonic Vibrational Polaritons of Small Molecules in Cavities. *J. Chem. Phys.* **2021**, *154*, 104311.

(59) Frenkel, D.; Smit, B. *Understanding Molecular Simulation*; Elsevier: San Diego, CA, 2002.

(60) Miller, W. H.; Schwartz, S. D.; Tromp, J. W. Quantum Mechanical Rate Constants for Bimolecular Reactions. *J. Chem. Phys.* **1983**, *79*, 4889−4898.

(61) Chandler, D.; Wu, D. *Introduction to Modern Statistical Mechanics*; Oxford Univ. Press: Oxford, UK, 1987.

(62) F. Ribeiro, R.; Dunkelberger, A. D.; Xiang, B.; Xiong, W.; Simpkins, B. S.; Owrutsky, J. C.; Yuen-Zhou, J. Theory for Nonlinear Spectroscopy of Vibrational Polaritons. *J. Phys. Chem. Lett.* **2018**, *9*, 3766−3771.

(63) Qiu, L.; Mandal, A.; Morshed, O.; Meidenbauer, M. T.; Girten, W.; Huo, P.; Vamivakas, A. N.; Krauss, T. D. Molecular Polaritons Generated from Strong Coupling between CdSe Nanoplatelets and a Dielectric Optical Cavity. *J. Phys. Chem. Lett.* **2021**, *12*, 5030−5038.

(64) Coles, D. M.; Michetti, P.; Clark, C.; Tsoi, W. C.; Adawi, A. M.; Kim, J.-S.; Lidzey, D. G. Vibrationally Assisted Polariton-relaxation Processes in Strongly Coupled Organic-semiconductor Microcavities. *Adv. Funct. Mater.* **2011**, *21*, 3691−3696.

(65) del Pino, J.; Schröder, F. A. Y. N.; Chin, A. W.; Feist, J.; Garcia-Vidal, F. J. Tensor Network Simulation of Non-Markovian Dynamics in Organic Polaritons. *Phys. Rev. Lett.* **2018**, *121*, 227401.

(66) Grote, R. F.; Hynes, J. T. The Stable States Picture of Chemical Reactions. Ii. Rate Constants for Condensed and Gas Phase Reaction Models. *J. Chem. Phys.* **1980**, *73*, 2715−2732.

(67) Pollak, E. Theory of Activated Rate Processes: A New Derivation of Kramers' Expression. *J. Chem. Phys.* **1986**, *85*, 865−867.

(68) Eyring, H. The Activated Complex in Chemical Reactions. *J. Chem. Phys.* **1935**, *3*, 107−115.

(69) Slater, N. B. New Formulation of Gaseous Unimolecular Dissociation Rates. *J. Chem. Phys.* **1956**, *24*, 1256−1257.